Article

Cell Reports

Adaptation without Plasticity

Graphical Abstract

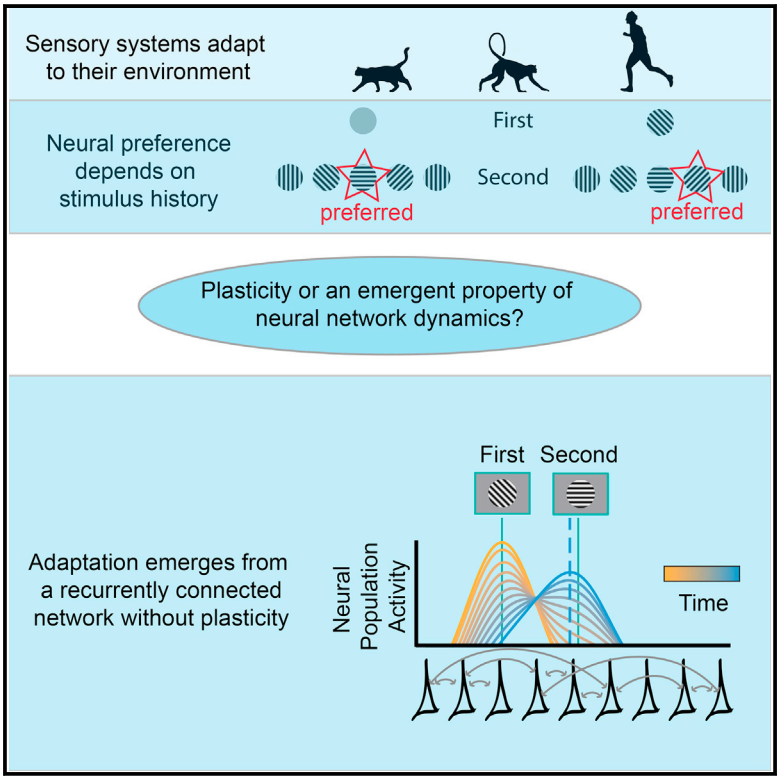

Authors

Maria del Mar Quiroga, Adam P. Morris, Bart Krekelberg

Correspondence

bart@vision.rutgers.edu

In Brief

Many sensory neurons adapt their response properties to recent input. This may enhance detection or discriminability of similar sensory inputs. del Mar Quiroga et al. show that this ability does not require neural plasticity, but emerges naturally from the dynamics of a recurrently connected network of neurons.

Highlights

- Plasticity is not necessary to explain short-term sensory adaptation
- Sensory adaptation can emerge from the dynamics of recurrent networks
- Fast neurons can have slow dynamics when connected recurrently
- Recurrent connections allow a network to store recent, contextual information

del Mar Quiroga et al., 2016, Cell Reports *17*, 58–68
September 27, 2016
http://dx.doi.org/10.1016/j.celrep.2016.08.089

CellPress

OPEN ACCESS
CellPress

Cell Reports
Article

Adaptation without Plasticity

Maria del Mar Quiroga,[1,2] Adam P. Morris,[3] and Bart Krekelberg[1,4,*]
[1]Center for Molecular and Behavioral Neuroscience
[2]Behavioral and Neural Sciences Graduate Program
Rutgers University-Newark, Newark, NJ 07102, USA
[3]Department of Physiology, Neuroscience Program, Biomedicine Discovery Institute, Monash University, Clayton, VIC 3800, Australia
[4]Lead Contact
*Correspondence: bart@vision.rutgers.edu
http://dx.doi.org/10.1016/j.celrep.2016.08.089

SUMMARY

Sensory adaptation is a phenomenon in which neurons are affected not only by their immediate input but also by the sequence of preceding inputs. In visual cortex, for example, neurons shift their preferred orientation after exposure to an oriented stimulus. This adaptation is traditionally attributed to plasticity. We show that a recurrent network generates tuning curve shifts observed in cat and macaque visual cortex, even when all synaptic weights and intrinsic properties in the model are fixed. This demonstrates that, in a recurrent network, adaptation on timescales of hundreds of milliseconds does not require plasticity. Given the ubiquity of recurrent connections, this phenomenon likely contributes to responses observed across cortex and shows that plasticity cannot be inferred solely from changes in tuning on these timescales. More broadly, our findings show that recurrent connections can endow a network with a powerful mechanism to store and integrate recent contextual information.

INTRODUCTION

Neurons in primary visual cortex (V1) are strongly tuned to the orientation of visual stimuli within their receptive fields (Hubel and Wiesel, 1962). Some debate persists surrounding how neurons acquire this tuning (Ferster and Miller, 2000), including the relative influences of feedforward versus recurrent inputs (Priebe and Ferster, 2008; Sompolinsky and Shapley, 1997). However, it is widely accepted that initial tuning is determined by selective pooling of inputs from the lateral geniculate nucleus (LGN) and then further modified (sharpened, made contrast invariant) by the recurrent cortico-cortical connections that account for up to half of the inputs to V1 neurons (Chung and Ferster, 1998).

Several studies have shown that the orientation preference of single neurons is altered by exposure to oriented stimuli (Clifford et al., 2001; Dragoi et al., 2000, 2002; Felsen et al., 2002; Müller et al., 1999; Patterson et al., 2013, 2014; Wissig and Kohn, 2012). These alterations in neural responses have been linked to perceptual phenomena such as the tilt after-effect (TAE), where adaptation produces a "repulsive" shift in orientation perception (i.e., perception of orientation is biased away from that of the adaptor stimulus) (Gibson and Radner, 1937). Remarkably, neural adaptation can be observed even when the adapting stimulus is presented for only a fraction of a second (Felsen et al., 2002; Müller et al., 1999). Analogous adaptation effects are found in all sensory brain areas and are thought to provide a functional benefit by enhancing discriminability of stimuli that are prevalent in the environment (Krekelberg et al., 2006b; Kristjánsson, 2011; Müller et al., 1999; Schlack et al., 2007) or by increasing detectability of rare stimuli (Clifford et al., 2001; Dragoi et al., 2002).

Crucially, adaptation and its associated benefits are commonly thought to arise from changes in the intrinsic properties of neurons or the efficacy of synaptic inputs (Felsen et al., 2002; Teich and Qian, 2003). Here, however, we evaluated and confirmed an alternative explanation: that short-term adaptation (and therefore its potential associated benefits) are emergent properties of processing sequential stimuli within a recurrent neural network.

We first show that a well established recurrent network model of orientation tuning (Carandini and Ringach, 1997; Somers et al., 1995; Teich and Qian, 2003) quantitatively captures changes in orientation tuning curves that have previously been observed in cat (Felsen et al., 2002) and macaque (Patterson et al., 2013) primary visual cortex, without the need for any changes in intrinsic properties or synaptic connectivity. Second, we show that these adaptation effects, including the non-stationarity of tuning, result from slow dynamics that emerge from the recurrent interactions among a population of fast neurons. Given the ubiquity of recurrent connections in cortex, such slow dynamics and their influence on neuronal tuning are predicted to also play a substantial role beyond primary visual cortex.

RESULTS

We studied the dynamics of a recurrent network model of orientation tuning in primary visual cortex (Carandini and Ringach, 1997; Somers et al., 1995; Teich and Qian, 2003) (see Experimental Procedures). The main properties and biological plausibility of this model have been documented in previous studies (Carandini and Ringach, 1997; Somers et al., 1995; Teich and Qian, 2003). Briefly, the model consisted of a bank of V1 units,

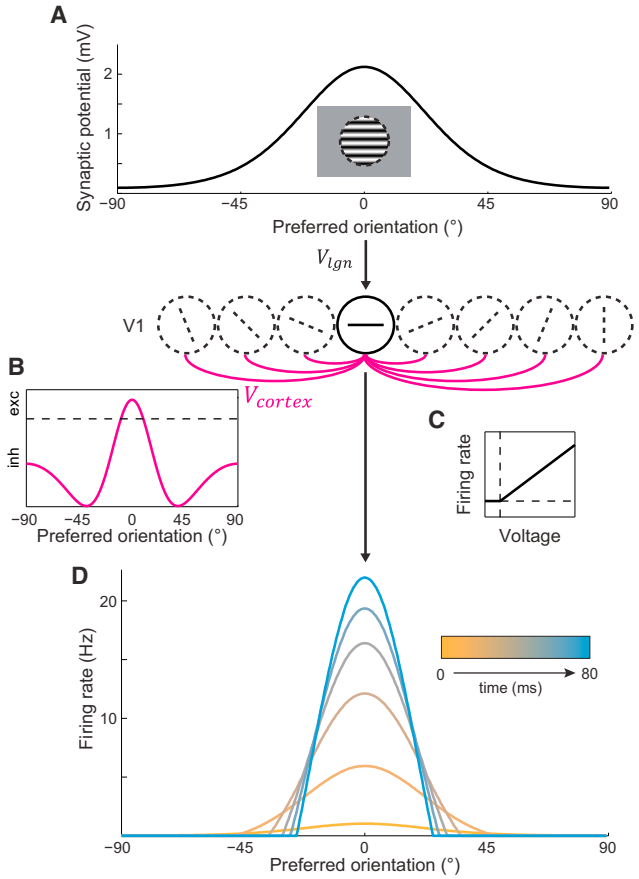

Figure 1. Response Dynamics in a Recurrent Model of Orientation Selectivity

(A) Thalamocortical input to each model neuron for a horizontal grating (0°; see inset) as a function of the neurons' preferred orientation.

(B) Intracortical connection profile for the neuron with preferred orientation 0°.

(C) Piecewise linear function that converts membrane potential to firing rate.

(D) Population response to a horizontal grating presented for 80 ms. The color represents time.

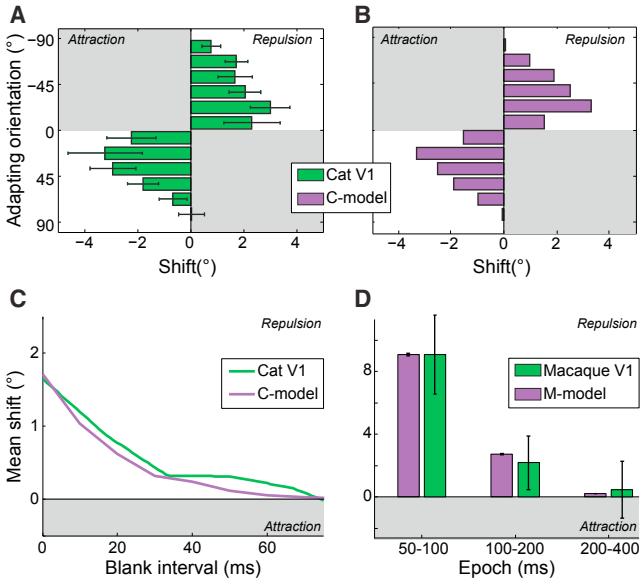

Figure 2. Population Dynamics Account for the Magnitude and Time Course of Tuning Curve Shifts Found in Cat and Macaque Visual Cortex

Grey background areas represent attractive shifts; white background repulsive shifts.

(A) Tuning curve shifts averaged over all recorded neurons (preferred orientation set to 0°) in cat V1 (Felsen et al., 2002). Error bars represent the SEM.

(B) Tuning curve shifts for the C-model neuron with preferred orientation 0°.

(C) Time course of tuning curve shifts for the cat data corresponding to (A) and the C-model.

(D) Time course of tuning curve shifts averaged over all recorded neurons from macaque V1 (Patterson et al., 2013) and the M-model. Error bars represent 95% confidence intervals. This figure shows that the recurrent network model can capture the adaptation effects observed in both cat and macaque V1.

each with a different preferred stimulus orientation determined by their weakly tuned feedforward input from a thalamic layer (Figure 1A). Lateral connectivity for each neuron was modeled as the difference of two von Mises functions, one representing excitatory connections and the other inhibitory. For appropriate parameter choices, this results in a typical "Mexican hat" profile (Figure 1B). The membrane potential of each model neuron was converted to an instantaneous firing rate using a piecewise linear function that determined response gain (Figure 1C). Importantly, the model parameters were fixed over time and did not implement any form of intrinsic plasticity, such as changes in synaptic strength or response gain.

Adaptation without Plasticity

We predicted that slow timescales emerging from the attractor dynamics of a recurrently connected network could produce adaptation-like phenomena. We investigated this by examining the extent to which the recurrent model could mimic previously reported adaptation effects found in cat (Felsen et al., 2002) and macaque (Patterson et al., 2013) primary visual cortex.

The Felsen et al. (2002) study measured tuning curves during sequences of very brief (17–25 ms) oriented stimuli in cat V1 (see Experimental Procedures; data replotted in Figures 2A and 2C). Their neurons showed repulsive effects on tuning curves, such that the preferred orientation of the neuron shifted away from the orientation of the preceding visual stimulus (the "adaptor"). The effect was greatest for adaptor orientations on the flanks of the tuning curves, leading to a biphasic pattern of shifts (Figure 2A). These effects decayed rapidly with the introduction of a blank interval between the adaptor and test orientation (Figure 2C). We used these experimental data, plus general knowledge about the properties of V1 neurons, to constrain the free parameters of the model. Specifically, the model parameters had to satisfy two criteria. First, the model had to produce V1-like responses to oriented stimuli presented in isolation (i.e., plausible peak firing rate, tuning bandwidth, and time-to-peak; see Experimental Procedures). Second, the responses to sequential pairs of oriented stimuli had to reproduce as closely as possible the adaptation pattern and dynamics observed by Felsen et al. (2002) (i.e., Figures 2A and 2C). We refer to this parametrization as the "C-model" (i.e., the Cat V1 model). We found that the

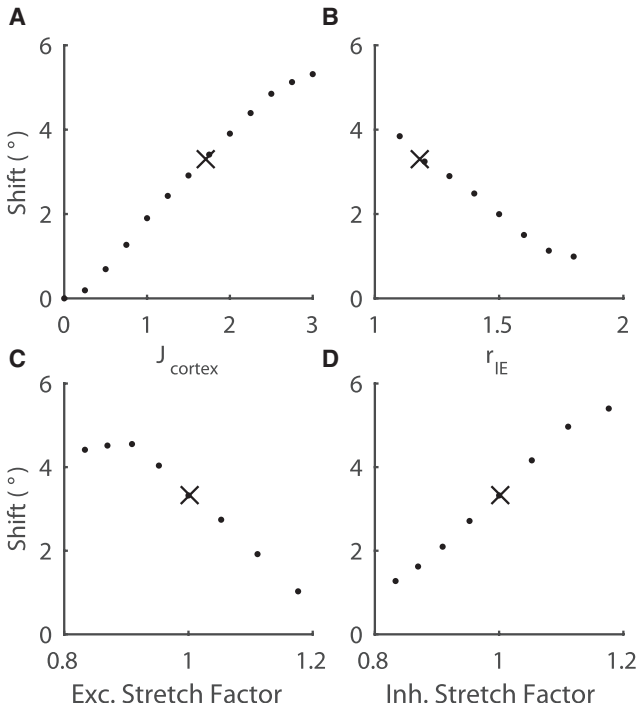

Figure 3. Systematic Exploration of Critical Network Parameters

For each panel all model parameters except for the one on the horizontal axis were fixed to those of the C-model. We simulated an adaptation protocol with adapters ranging from −90° to 0° and determined the maximum shift across adapters.

(A) Tuning curve shift as a function of the strength of intracortical connections (J_{cortex}).

(B) Tuning curve shift as a function of the balance between inhibition and excitation (r_{IE}).

(C) Tuning curve shift as a function of the tuning width of the excitatory connections. The horizontal axis corresponds to the factor by which the connection profile was broadened (stretch factor >1) or narrowed (stretch factor <1) compared to those in the C-model (Experimental Procedures).

(D) Tuning curve shift as a function of the tuning width of the inhibitory connections. The crosses show the shift observed in the C-model without any parameter changes. This figure shows that tuning curve shifts were largest when the intracortical connections were strong, when excitation and inhibition were balanced (r_{IE} close to 1), when the excitatory connections were narrow, or when the inhibitory connections were broad. See also Figure S1.

C-model captured the direction, magnitude, and time course of the tuning curve shifts in cat visual cortex (Figures 2B and 2C). That is, it exhibited adaptation behavior that would traditionally be held as evidence for rapid neural plasticity. In the model, however, adaptation occurred without plasticity.

We then investigated whether the same model architecture could also capture the tuning curve shifts reported for *macaque* V1 under different experimental conditions (Patterson et al., 2013). Patterson et al. (2013) used longer adaptation and test stimuli (400 ms each) and found larger and longer-lasting (~200 ms) repulsive shifts than those found in the cat. Following the same procedures as before to determine the free model parameters, we found that recurrent network dynamics also accounted for the adaptation effects in macaque visual cortex (M-model; Figure 2D).

Inspired by the substantial difference in magnitude and dynamics between the C- and M-model, we also performed a wider parameter exploration (i.e., not tailored to fit any specific experimental data set; see Experimental Procedures) and found that the model architecture could generate very large (~10°) and long-lasting (~1 s) tuning curve shifts (see Figure S1), while still maintaining basic tuning properties for isolated stimuli consistent with recordings in V1. A comparison of the recurrent connectivity between the various models suggests that the strength of the lateral connectivity was a significant contributing factor to the magnitude and decay time course of the adaptation dynamics. For example, the C-Model, in which the tuning curve shifts decayed rapidly, had relatively weak intracortical connections, whereas the model that had large and long-lasting shifts ("slow model") had strong connections (Figure S1). We investigated this systematically by perturbing the parameters of the C-model and determining the size of the maximum shift attained. Figures 3A and 3B confirm that a stronger overall strength of lateral connectivity (increased J_{cortex}) increased the magnitude of the tuning curve shifts, while an increase in the strength of inhibition relative to excitation (i.e., larger r_{IE}) decreased the size of the tuning curve shifts. We also explored the influence of the tuning of the recurrent connections (i.e., the shape of the Mexican hat) by narrowing or broadening the weight profiles (Experimental Procedures). Figure 3C shows that broader tuning of the excitatory connections led to smaller tuning curve shifts. Figure 3D shows the equivalent result for the tuning of inhibitory connections; broader tuning of the inhibitory connections led to larger tuning curve shifts.

Taken together, these findings demonstrate that a network of neurons with fast membrane time constants (τ = 15 ms) can, depending on the strength and shape of its recurrent connections, produce surprisingly slow and large adaptation effects. Importantly, the responses of the model neurons to single stimuli were brisk and compatible with experimental data (see Figure 1 and Experimental Procedures). This analysis provides a proof of principle, the model can reproduce many experimental findings without plasticity. Next, we use the model to unpack the network dynamics and understand how this happens. Unless otherwise specified, the results shown in figures were obtained with the C-model, although qualitatively similar results follow from the M-model.

Responses to a Single Visual Stimulus

When presented with a horizontal grating (0°), the model initially showed a broadly distributed response across neurons with different preferred orientations, as has been observed experimentally (Benucci et al., 2009; Carandini and Ringach, 1997). Over time, the population response increased and sharpened, converging to a hill-like shape with a width of ~32° (Figure 1D). This steady-state response continued as long as the stimulus was present. By construction (see Experimental Procedures), these response dynamics are within the range observed experimentally.

To investigate the role of recurrent connectivity on neural response dynamics, we modified the strength of the intracortical connections and examined responses of the unit that preferred horizontal orientations to a single grating of that orientation. A

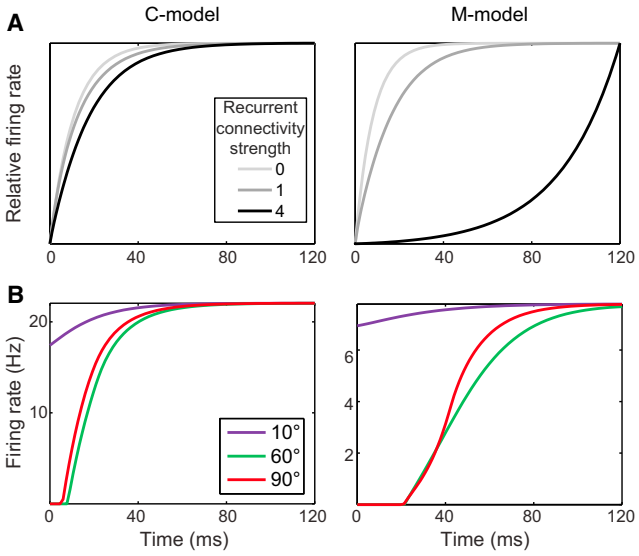

Figure 4. Cortical Connectivity and Stimulus History Affect Response Dynamics

Left panels correspond to the C-model, right panels to the M-model.

(A) Peak normalized firing rate after stimulus onset shown for networks with absent ($J_{cortex} = 0$; light gray curve), intermediate (medium gray curve), and strong (black curve) recurrent connectivity.

(B) Response of the model neuron with preferred orientation 0° to the onset of a horizontal grating (time = 0) preceded by one of three adaptor orientations: 10° (purple), 60° (green), or 90° (red).

purely feedforward variant (recurrent inputs fixed at zero) reached steady state after ~40 ms. Recurrent variants, in contrast, had convergence times that were substantially longer (150%) and increased with the strength of intracortical connectivity (Figure 4A, left). These effects were even stronger in the M-model (Figure 4A, right), and the model in which the intracortical connection strength was 4-fold stronger than the M-model failed to converge entirely (black curve). Thus, response dynamics were not only determined by the intrinsic properties of individual neurons (which were fixed in these simulations), but also by their connectivity.

Responses to Sequential Stimuli

To understand why tuning curves shift after recent exposure to an oriented stimulus, we further examined single unit and population responses to sequential pairs of gratings. The first grating (i.e., the adaptor) was presented until the network converged. Of key importance is what happened in the network when the stimulus was then switched to a new orientation (i.e., the "test"). Interestingly, the network dynamics depended on the difference in orientation between the two successive gratings. For instance, when a 0° test grating was preceded by a nearby adaptor orientation (10°), the neuron that preferred 0° gratings reached a steady-state response 40 ms after the onset of the second grating (Figure 4B, left, purple curve). When preceded by a distant orientation (60° or 90°), however, the same neuron required ~50% more time to converge (Figure 4B, left, green and red curves). The M-model had even slower dynamics (Figure 4B, right).

The response to test stimuli similar to the adaptor orientation is nimbler because the adaptor response closely resembles that of the test and thus gives it a head start at the beginning of the test period. While this result is intuitive, we show below that these interactions generate complex dynamics in the population and bias the representation of orientation when stimuli change rapidly.

We examined the population dynamics by simulating the presentation of pairs of gratings (adaptor/test) and by varying the duration of both stimuli. After the onset of the test grating in a −45°/0° pair with 80 ms presentation time per grating, the population activity declined from its peak at −45° and gradually shifted to reestablish itself around the neurons preferring 0° (Figure 5A). For pairs with similar orientations (−20°/0°), population activity resembled a traveling wave shifting between the presented orientations (Figure 5C). Finally, when the pairs were orthogonal, (−90°/0°; Figure 5D), activity collapsed around −90° as it resurfaced around 0°. Such dynamic patterns of network activity have been observed experimentally using voltage sensitive dye imaging in the cat visual cortex (Benucci et al., 2009).

Thus, for 80 ms presentations, the population exhibited complex transitions from adaptor to test, but nevertheless represented orientation accurately by the end of the test period. Crucially, however, this was not the case for shorter presentation times because the transitions were interrupted midway. As a consequence, the peak of the population response at the end of the test stimulus presentation could be biased toward the neurons that preferred the adaptor (Figures 5B and 5C). The size of this bias depended on the orientation difference between the adaptor and the test grating in a non-monotonic fashion (compare [B–D] in Figure 5). This analysis shows that the responses of neurons in the recurrent network were not only determined by its immediate sensory input, but also by the temporal context provided by the preceding inputs. In other words, the recurrent network demonstrated a property commonly termed adaptation.

To allow a direct comparison with experimental results (which typically report tuning curves of individual neurons rather than population responses), we simulated neural responses in a standard orientation tuning protocol (i.e., presenting test stimuli in temporal isolation) and in an adaptation protocol in which the test stimulus was preceded by an adaptor oriented 20° away from horizontal (Figure 6A). In both cases, we measured the tuning curve of the neuron whose nominal preferred orientation was horizontal (0°). By definition, the tuning curve in the standard protocol had a peak at the 0° orientation (Figure 6B, gray curve). In the adaptation paradigm, however, the presence of a hill of activity generated by the adaptor (Figure 5) resulted in, somewhat counterintuitively, a shift of the tuning curve away from the adaptor orientation (Figure 6B, black curve). Consistent with tuning curve dynamics in primary visual cortex (Dragoi et al., 2000), the shift in the adapted tuning curve is dominated by an increased response to orientations in the non-adapted flank (see Discussion). As shown in Figure 2B, the direction and magnitude of these tuning curve shifts depended on the orientation of the adaptor, with a biphasic, repulsive pattern, consistent with electrophysiological recordings (Felsen et al., 2002).

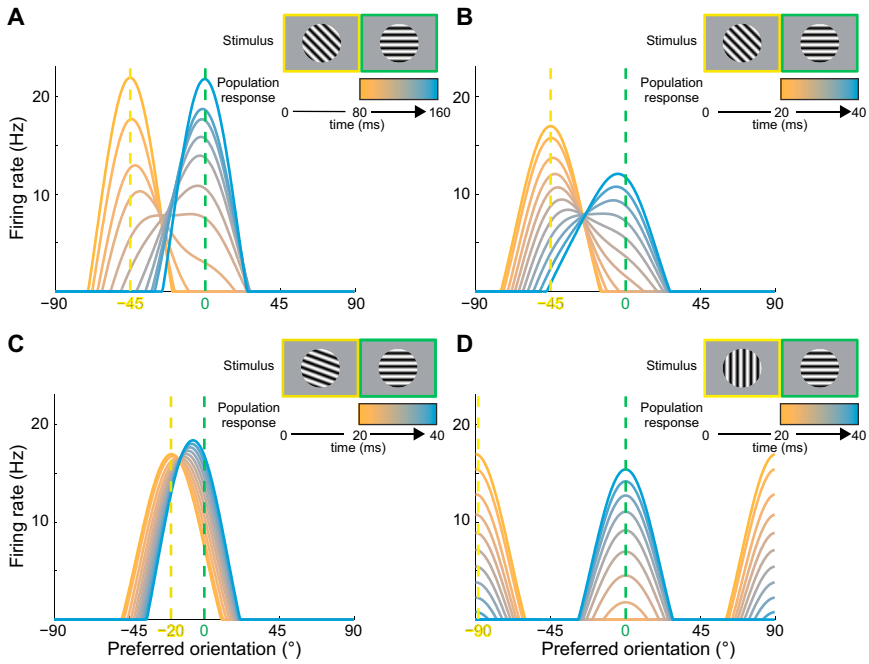

Figure 5. Population Responses in an Adaptation Paradigm

Each panel shows the response to a horizontal grating that was preceded by an adaptor orientation (color represents time after the onset of the horizontal grating).

(A) Response to an 80 ms presentation of a stimulus with orientation 0°, preceded by an 80 ms presentation of a stimulus oriented at −45° (−45°/0° pair). The final population response to the second 0° stimulus (160 ms) peaks at the neuron with preferred orientation 0°.

(B) Response to a −45°/0° pair with each grating presented for 20 ms.

(C) Response to a 20 ms −20°/0° pair.

(D) Response to a 20 ms −90°/0° pair. The short stimulus presentations bias the population response for some (B and C), but not other sequences (D).

Mechanism

To gain insight into the principles and mechanisms underlying tuning curve shifts, we zoomed in on the neural responses in a specific simulated experiment. We show the results of the M-model, but analogous results were found in all models. Our goal is to understand how the tuning curve shifts arise from the recurrent network dynamics. We focus on the neuron with a preferred orientation of 0° (the 0° neuron, for short) and simulate an adaptation paradigm with a −25° adaptor presented for 50 ms. In the M-model, this would result in a ~10° repulsive shift in the orientation tuning curve measured with 50 ms test stimuli. This statement about the tuning curve is equivalent to the statement that, averaged over the first 50 ms of stimulus presentation, a 10° test stimulus will generate a larger response than the 0° test stimulus. How does a non-preferred stimulus generate a larger response than the preferred stimulus?

The response of each neuron is determined by the combination of feedforward and recurrent input (Equations 1 and 2). Figure 7A shows the feedforward input to the 0° neuron (red curve) as a function of test stimulus orientation. Of course, the largest feedforward input to the 0° neuron occurs when the test stimulus orientation is 0°. Without the presentation of the adaptor (dashed green curve), the recurrent input to the 0° neuron is also largest when the stimulus is 0°. After adaptation, however, the largest (least inhibitory) recurrent input to the 0° neuron occurs for test stimuli with orientations larger than 0° (solid green curve). This implies that, following adaptation, the 0° neuron can respond more to a 10° test than to its nominally preferred orientation of 0°, provided that the recurrent input is sufficiently strong. This recurrent input arises from neurons within the hill of population activity generated by the adaptor. Understanding the dynamics of this hill of population activity is therefore critical to understanding tuning curve shifts.

Soon (15 ms) after the onset of the test stimulus, the V1 population activity mainly reflects the reverberating activity caused by the adaptor (Figure 7B, blue lines). The peak of activity is close to the neuron whose preferred orientation matches the −25° adaptor (indicated by the arrow). Consider what happens to this hill of adaptor-related population activity 15 ms after presentation of the 10° test. The 10° test provides its strongest feedforward drive to the neurons on the right flank of the hill and only weak input to the left flank of the hill (Figure 7B, right axis, red dashed line). As a result, the total input to some neurons on the right flank rises above threshold, while some of the neurons on the left flank drop below threshold. This implies that the hill of activity moves rightward. After moving to the right, its right flank receives even more and its left flank even less feedforward input from the 10° test. This results in further rightward movement of the hill (Figure 7C, dashed line).

The presentation of a 0° test stimulus results in a qualitatively similar rightward movement of the hill of adaptor-related population activity (Figure 7C, solid blue line). However, compared to the 10° test, the 0° test provides more feedforward drive to the center and left flank and less drive to the right flank of the hill (Figure 7B, compare red solid and dashed curve). Therefore, the hill moves more slowly after the presentation of the 0° test (Figure 7C, solid line). Importantly, there is a substantial period during which the hill is closer to the 0° neuron in trials with a 10° test, than in trials with a 0° test (Figure 7C, green shaded area).

Because only spiking neurons provide recurrent input to other neurons, all recurrent input arises from the hill of population activity. Figure 7B shows the hill of activity 15 ms after test stimulus onset. As explained above and shown in Figure 7C, the hill has shifted more to the right after the 10° test than after the 0° test (compare dashed with solid blue curve). Due to the Mexican hat shape of the intracortical weights, neurons with preferred orientation close to the hill receive net recurrent excitation (above the horizontal black dashed line representing 0 mV), while those further away receive net recurrent inhibition (below the

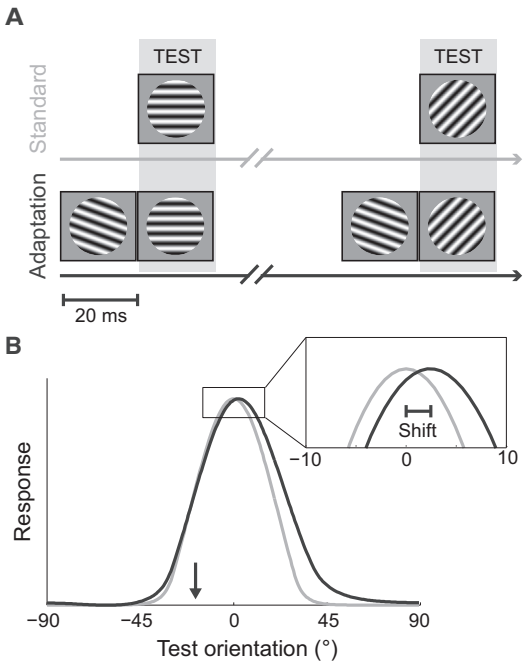

Figure 6. Recurrent Network Dynamics Generate Repulsive Tuning Curve Shifts in an Adaptation Protocol

(A) Standard and adaptation orientation tuning protocols.

(B) Peak normalized tuning curves for a neuron that prefers horizontal gratings obtained under the standard (gray) and adaptation (black) protocol. In the adaptation protocol, the tuning curve peaked at 3°. In other words, the −20° adaptor (arrow) induced a repulsive shift in the tuning curve.

black dashed line). Because the hill generated by the 10° test (Figure 7B, dashed blue curve) is closer to the 0° neuron than the hill generated by the 0° test (solid blue curve), the net recurrent input to the 0° neuron is larger after the presentation of the 10° test (dashed green curve) than after the presentation of the 0° test (solid green curve). This additional recurrent input from the hill of population activity that was created by the adaptor generates the larger response to the 10° than the 0° test stimulus and is therefore responsible for the shift of the tuning curve.

Figure 7D shows how this process unfolds over time by looking specifically at the input and output of the 0° neuron. At t = 50 ms, the adaptor (−25°) is replaced by the test (solid lines = 0° test and dashed lines = 10° test). The feedforward input to the 0° neuron is larger for the 0° test than the 10° test (red lines). The recurrent input, however, is larger for the 10° than the 0° stimulus (green lines). Initially this difference is small, but it grows over time because the hill of population activity moves rightward faster in the 10° trials than in the 0° trials (see Figure 7C). The dashed blue line shows the consequence; the neuron's response to the 10° test starts slightly lower (less feedforward input), but rapidly catches up and then overtakes the response to the 0° test stimulus (more net recurrent excitation). At that time, the 0° test stimulus no longer generates the largest response; it is no longer the preferred orientation, and hence, the tuning curve of the 0° neuron is repulsed from the −25° adaptor, toward 10°.

This description ignores several additional changes that occur at the same time. One important addition is that, given enough time and a constant test stimulus, the hill of population activity inevitably marches toward its final state in which the peak is centered on the neuron with the preferred orientation that matches the test stimulus. At t∼135 ms (i.e., 85 ms after test stimulus onset), the population peak is at equal distance from the 0° neuron in the two test conditions (Figure 7C). At this time, the recurrent excitation to the 0° neuron is equal in both conditions (i.e., the green curves in panel D cross over). From then onward, both the feedforward and recurrent input to the 0° neuron are maximal for the 0° stimulus, the response to the 0° stimulus becomes stronger than the response to the 10° stimulus (solid blue line crosses dashed blue line), and the preferred orientation of the 0° neuron again matches the nominal 0°.

This mechanism explains several salient experimentally observed properties of tuning curve shifts. First, tuning curve shifts are repulsive. The reason for this is that only test orientations to the right of 0° (i.e., the preferred orientation of the neuron under study) move the population activity toward the 0° neuron more and faster than the test orientation that matches the preferred orientation. Therefore, only those stimuli can generate more recurrent excitation to the 0° neuron, and only those orientations can (temporarily) generate a larger response than the nominally preferred orientation.

Second, this mechanism explains why the largest tuning curve shifts are found for adapters close to the flank of the tuning curve. This occurs because the additional recurrent drive generated by a non-preferred orientation results from the hill of population activity moving through the 0° neuron. If the hill of activity starts very close to the 0° neuron (i.e., after an adaptor close to 0°), the relative advantage of the 10° test compared to a 0° test is small and short-lived. If, on the other hand, the hill of activity starts far away from the 0° neuron (i.e., after an adaptor to the left of the flank), the population activity dynamics no longer resemble a moving hill, but two hills that wax and wane without traveling through the network (e.g., Figure 5D).

Finally, this mechanism also explains the role of the critical model parameters (Figure 3). Stronger recurrent excitation increases the influence of the hill of population activity. Hence, tuning curve shifts are large when recurrent connections are strong (J_{cortex} large; Figure 3A) and small when inhibition is strong compared to excitation (r_{IE} large; Figure 3B). The width of the hill of population activity determines the difference in recurrent excitation generated by two test stimuli; broad hills lead to small differences, while narrow hills lead to large differences. This explains the role of the excitatory and inhibitory tuning (Figures 3C and 3D); broader excitatory tuning (or narrower inhibitory tuning) leads to broader hills of population activity and smaller tuning curve shifts (see also Figure S2).

DISCUSSION

We found that recurrent network dynamics can give rise to repulsive shifts in tuning curves that mimic those observed experimentally in adaptation studies of primary visual cortex. Specifically, model neurons shifted their preferred orientation away from that of an adapting stimulus for up to ∼1 s (Figure S1). This effect

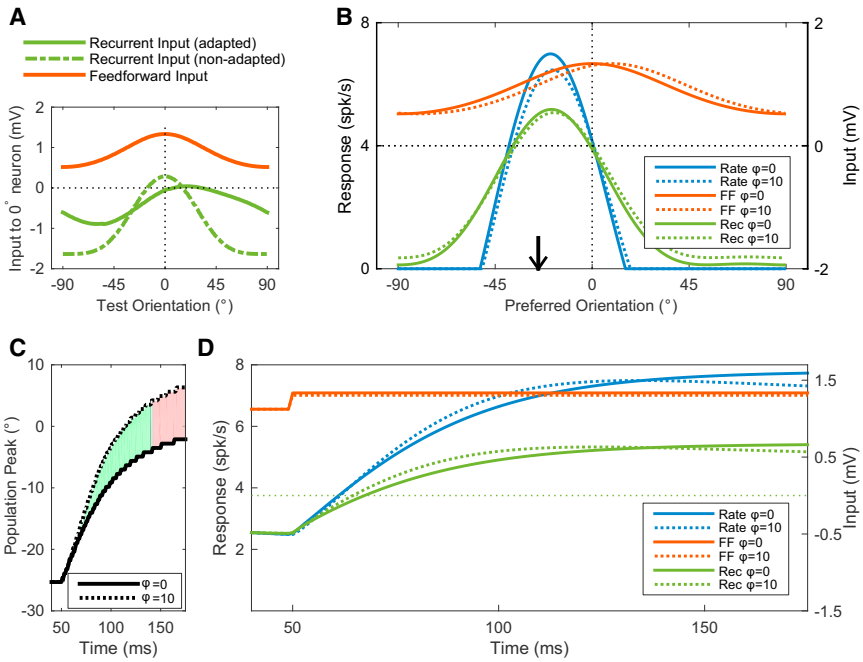

Figure 7. Mechanisms

Simulation of an adaptation protocol in the M-model. An adaptor (−25°) was presented to the M-model for 50 ms, followed by test stimuli of varying orientations for 125 ms.

(A) A snapshot of the feedforward and recurrent input to the 0° neuron at t = 65 ms as a function of test orientation.

(B) Snapshot of the population spiking activity (left axis) and input (right axis) at t = 65 ms. The black arrow represents the adaptor orientation. The solid lines correspond to a trial with a 0° test stimulus, and the dashed lines correspond to a trial with a 10° test stimulus.

(C) Time course of the peak of population activity when the 0° (solid) or 10° (dashed) test stimulus is presented. The green (red) shaded area shows the period during which the 0° neuron receives more (less) recurrent input from the 10° test than the 0° test.

(D) Time course of the response of the 0° neuron. The conventions are as in (B). feedforward input: FF, recurrent input: Rec, orientation of the test stimulus: φ. For details, see main text.

was a direct consequence of an interaction between the changing sensory environment and the dynamics of the network and not from changes in the properties of individual neurons or their synaptic connections. In other words, the model neurons demonstrated adaptation without plasticity. This shows that one cannot infer plasticity from adaptation, and that recurrent connections can result in slow dynamics that integrate temporal context, or stimulus history, into the neural response to ongoing input.

Dynamics versus Plasticity

By constructing a model without plasticity, we isolated the role of recurrent connectivity and showed how recurrent connections contribute to adaptation. In the brain, these recurrent network dynamics likely interact with other mechanisms that affect the dynamic response of neurons. At the shortest timescale, this can include the non-linear interaction among multiple stimulus features that results in rapid gain control (Borst et al., 2005), while at the timescale of s to min one would expect additional contributions from changes in intrinsic properties of single neurons (Sanchez-Vives et al., 2000) or the strength of synaptic connections between neurons (Yao and Dan, 2001). Nevertheless, the model quantitatively captures a large set of previously published experimental findings and makes testable predictions about the relation between population activity and single neuron responses in an adaptation paradigm (Figure 7). Most importantly, however, the model provides a conceptually unique, yet parsimonious, interpretation of dynamic changes in tuning.

The experimental finding of a repulsive shift in tuning following short-term adaptation is robust across studies, species, and recording sites (Dragoi et al., 2000, 2002; Felsen et al., 2002; Müller et al., 1999; Patterson et al., 2013, 2014; Wissig and Kohn, 2012). However, the dynamics of these shifts as well as the details of tuning curve shapes differ significantly across studies and sites. Because previous studies assumed all tuning curve changes were caused by short-term plasticity, such differences could only be interpreted as resulting from differences in plasticity across species or across recording sites. The recurrent network model, however, offers the alternative interpretation that differences in the magnitude or time course observed experimentally may be due to differences in the strengths or spatial profiles of the recurrent connectivity.

There is ample evidence that tuning curve shifts vary across sites in the same animal. This is implicit in the variability observed in many studies, but Dragoi et al. (2000) also report systematic changes in V1: repulsive shifts are larger near the pinwheels of orientation maps than in an iso-orientation domain. Dragoi et al. (2000) attributed these differences to a larger degree of plasticity near pinwheels, but our model now offers the alternative interpretation that recurrent connectivity is different near pinwheels. For instance, stronger excitatory connections or more broadly tuned inhibitory connections could explain the larger tuning curve shifts (Figure 3). Given that more neurons with different preferred orientations are available at a short cortical distance for a neuron in a pinwheel than for a neuron in an iso-orientation domain, we believe that this is a reasonable and attractive alternative explanation. Connectivity differences between the sites that were sampled in the monkey compared to those sampled in the cat could also explain the differences between the M- and C-models (rather than a true species difference). An intriguing corollary of this is that it may be possible to invert this relationship and infer local connectivity by recording large sets of dynamic responses to stimulus sequences.

Timescales of Adaptation

Many phenomena, at virtually any timescale, are referred to as adaptation. We do not claim they can all be explained by the

single mechanism—recurrent network dynamics—that we focused on here. Our claim is merely that recurrent network dynamics can contribute in a significant manner to sensory adaptation at timescales of at least several hundreds of milliseconds. This is important because this potential contribution has not been considered in previous work on adaptation, and because this timescale is ecologically highly relevant given that eye movements cause entirely new input to arrive in visual cortex every few hundred milliseconds (Ibbotson and Krekelberg, 2011).

Even though recurrent network dynamics are unlikely to affect responses on timescales beyond s, they can nevertheless confound the interpretation of typical long-term adaptation paradigms. The reason for this is that experimental paradigms that quantify long-term adaptation typically briefly repeat the adaptor just before the test (the so-called "top-up design"). As a consequence, such measurements of long-term adaptation (which likely involves some kind of plasticity) may be confounded with the more short-lived effects reported here (dynamics). This may offer an explanation for some of the contradictory reports found in the fMRI adaptation literature (Kar and Krekelberg, 2016; Krekelberg et al., 2006a); future studies could remove this confound by introducing a substantial temporal delay between adaptor and test presentation.

Plausibility

As shown in previous studies, firing rate models reproduce many of the features of more complex, spiking neuron models and capture many of the orientation tuning properties observed in V1 (Carandini and Ringach, 1997; Somers et al., 1995; Teich and Qian, 2003). We focused on a firing rate model because it allowed us to perform parameter optimization with an eye to reproducing the specific experimental data sets obtained in cat and macaque visual cortex. By construction (Experimental Procedures), the model parameters we used resulted in neurons with firing rates, response dynamics, and tuning curve widths that were all within the range typically observed in the brain. Moreover, although quantitative measures of connectivity in visual cortex are difficult to obtain, the connectivity in the model qualitatively matches estimates of connectivity in primary visual cortex (Kaschube, 2014; Ko et al., 2011; Michalski et al., 1983; Roerig and Chen, 2002). This too adds to the plausibility of the model.

Nevertheless, the model is a substantial simplification of biological reality. First, neurons in the brain are either excitatory or inhibitory, but units in our model can be both. To ensure that the observed tuning curve shifts are not an artifact of this simplification, we also implemented a model with distinct populations of excitatory and inhibitory units (E/I model; Ben-Yishai et al., 1997). This model reproduced our key findings and observations, including tuning curve shifts (see Figure S3). Second, the units in our model all have identical spatial receptive fields, while in the brain, neurons with separate spatial receptive fields interact. These center-surround, contextual, modulations affect orientation tuning (Angelucci and Bressloff, 2006; Gilbert and Wiesel, 1990; Shushruth et al., 2012), which can interact with adaptation (Wissig and Kohn, 2012), and contribute to other complex tuning properties (Richert et al., 2013; Schwabe et al., 2006).

The dynamics of models with multiple populations of interacting neurons, however, are substantially more complex than the single population model studied here (Ben-Yishai et al., 1997; Bressloff et al., 2000; Hansel and Sompolinsky, 1998; Wilson and Cowan, 1972). By analogy with our approach for simple adapt/test experimental protocols, it may be possible to use the dynamic responses to more complex spatio-temporal stimulus sequences to constrain the free (connectivity) parameters in such models. This approach, integrating tailored experimental data collection with these more complex dynamic models, may provide deeper insight into the function of the spatio-temporal interactions enabled by recurrent connectivity (Schwartz et al., 2007).

Recurrent Networks

Many aspects of sensory processing are captured more naturally in a recurrent than a feedforward network. We recently developed a recurrent network model for the detection of motion that capitalizes on this property. Standard motion models typically assume delay lines or postulate the existence of classes of neurons that are intrinsically slow or fast. In the recurrent network, however, these properties emerge from the network dynamics (Joukes et al., 2014). Other examples of the computational flexibility of recurrent networks include the selective amplification of noisy signals (Hahnloser et al., 2002) and the state-dependent processing of inputs (Rutishauser and Douglas, 2009). Our orientation model borrows principles of computation from each of these; the network dynamics lead to temporal interactions among stimuli, which result in selective amplification and state-dependent processing. These computations are likely to be useful beyond primary visual cortex, and our findings, therefore, highlight the general need to consider how recurrent connectivity imbues a network with a powerful and potentially multipurpose ability to compute complex functions of its inputs.

EXPERIMENTAL PROCEDURES

We implemented a recurrent model of orientation selectivity following the work of Carandini and Ringach (1997), Somers et al. (1995), and Teich and Qian (2003). The model consisted of coupled differential equations describing the membrane potential of N orientation selective primary visual cortex neurons (Figure 1). As a whole, the network represents a cortical hypercolumn (i.e., all N spatial receptive fields overlap), and all N neurons are identical except for their preferred orientation. The preferred orientations of the N model neurons were evenly distributed across all orientations (-90° to 90°), and we labeled each model neuron based on its preferred orientation θ. Each neuron was modeled as a single passive voltage compartment, whose membrane potential over time $V^\theta(t)$ obeyed the differential equation:

$$\tau \frac{dV^\theta}{dt} + V^\theta = V^\theta_{lgn} + V^\theta_{cortex}, \qquad \text{(Equation 1)}$$

where τ is the membrane time constant, V^θ_{lgn} the synaptic potential generated by the thalamocortical inputs to the model neuron, and V^θ_{cortex} is the net synaptic input to the neuron from its cortical neighbors (Carandini and Ringach, 1997; Teich and Qian, 2003).

The instantaneous firing rate for the neuron with preferred orientation θ at time t was calculated as:

$$R^\theta(t) = \alpha \max\left(V^\theta(t), 0\right), \qquad \text{(Equation 2)}$$

where $V^{\theta}(t)$ is the voltage of the neuron with preferred orientation θ at time t (see Figure 1C). This results in a mean firing rate model, with α the corresponding gain factor (i.e., increase in firing rate [Hz] for a 1 mV increase in the membrane potential). For simplicity, the neurons have zero spontaneous firing rate, and the membrane potential was measured relative to the spike threshold. In other words, a positive membrane potential results in spikes, whereas a negative membrane potential reflects a modulation for the model neuron below the spiking threshold, hence the zero on the right of Equation 2.

Our implementation is similar to the work of Carandini and Ringach (1997) and Teich and Qian (2003), except that we used von Mises functions to represent the thalamocortical input as well as the lateral connectivity in the network. Using this differentiable and circular function instead of the non-circular (truncated) Gaussians of previous studies improved the numerical behavior of the network and removed artifacts from the dynamics. For each model cortical neuron with preferred orientation θ, the input from LGN was a function of stimulus orientation ω and contrast c:

$$V^{\theta}_{lgn}(\omega, c) = cJ_{lgn} f\left(\omega \mid \theta, \kappa_{lgn}\right), \qquad \text{(Equation 3)}$$

where J_{lgn} represents the strength of the input and $f(\omega \mid \theta, \kappa_{lgn})$ is the von Mises distribution with period π, mean θ, and concentration κ_{lgn} (inversely related to the width; Figure 1A):

$$f(x \mid \mu, \kappa) = \frac{e^{\kappa \cos(2(x-\mu))}}{2\pi I_0(\kappa)}. \qquad \text{(Equation 4)}$$

$I_o(\kappa)$ is the modified Bessel function of order zero. For the results shown in the main text, we followed previous implementations and did not incorporate separate units to represent excitatory and inhibitory cells, but rather gave each model neuron the ability to produce both net excitation and inhibition (see Figure S3 for analogous results obtained in a model with separate excitatory and inhibitory populations).

Experimental studies have found that the probability of connection between two orientation selective neurons is not uniform. Instead, the probability of connection is highest for neurons with similar preferred orientation and decreases with increasing difference in preferred orientation (Ko et al., 2011; Michalski et al., 1983; Roerig and Chen, 2002). Based on these findings, we modeled both the excitatory (E^{θ}) and inhibitory (I^{θ}) connection profiles to the model neuron with preferred orientation θ as von Mises distributions in orientation space (see Equation 4):

$$E^{\theta}(\phi) = f(\phi \mid \theta, \kappa_E) \qquad \text{(Equation 5)}$$

$$I^{\theta}(\phi) = f(\phi \mid \theta, \kappa_I). \qquad \text{(Equation 6)}$$

When the inhibitory connection profile was (marginally) broader than the excitatory one $(\kappa_E > \kappa_I)$, the connection profile ($F^{\theta}(\phi)$; Figure 1B) had the typical Mexican hat shape:

$$F^{\theta}(\phi) = J_{cortex}\left(E^{\theta}(\phi) - r_{IE} I^{\theta}(\phi)\right). \qquad \text{(Equation 7)}$$

In this recurrent connection profile, J_{cortex} represents the strength of the cortical connections and r_{IE} the ratio of the strength of inhibition to the strength of excitation. The width of the excitatory and inhibitory profile is determined by the κ_E, κ_I, but their relation with the width of the profile is not intuitive. For instance, decreasing κ increases the width, but can also increase the offset of the profile. In the parameter exploration simulations (Figure 3), our goal was to determine how tuning curve shifts were affected by perturbations of intuitive measures of connectivity. Therefore, we kept κ_E, κ_I constant and manipulated the width by stretching (or compressing) the profiles by scaling the $(x - \mu)$ coordinate of the von Mises function (i.e., $(x-\mu) \rightarrow (x-\mu)/s$). The parameter s—the stretch factor—directly represents the influence on the width of the profile ($s > 1$: broadening and $s < 1$: narrowing).

At each point in time, the membrane potential for the neuron with preferred orientation θ induced by the recurrent input is a weighted sum of the firing rates of all neurons in the network (Equation 2):

$$V^{\theta}_{cortex}(t) = \sum_{\phi} F^{\theta}(\phi) R^{\phi}(t). \qquad \text{(Equation 8)}$$

The model and all simulations were implemented in MATLAB and solved numerically using *ode45*, an adaptive time step Runge-Kutta method. The number of model units in the network (N) was set to 256 and the stimulus contrast c was set to 50%.

Given our main purpose of studying temporal dynamics induced by recurrent connectivity, and unlike previous work, we explored model responses at every time point during the simulation as opposed to only the final steady-state responses. This allowed a direct comparison of the simulations with experimental data.

From Population Responses to Tuning Curves

The output of the model is the response of all neurons to a single stimulus (Equations 1 and 2). Lining up all model neurons on the x axis according to their preferred orientations and plotting the response of each one on the y axis, we obtain what we call the population response (Figure 1D). Electrophysiology experiments, on the other hand, typically report tuning curves of individual neurons: the response of a single neuron to all possible stimulus orientations. To obtain tuning curves for our model neurons, we simulated the population response to a range of stimulus orientations and extracted from each of these the response of one specific model neuron.

The tuning curves presented in Figure 6B were obtained following either a standard or an adaptation tuning protocol (Figure 6A). Mimicking the procedure in electrophysiological experiments, for the standard protocol, we presented one test orientation per trial and averaged the firing rate over the duration of the test stimulus. To preclude systematic interactions beyond the measurements in one trial, the response of each neuron was reset to the spontaneous firing rate at the end of the trial (experimentally, this would correspond to a long inter-trial interval). In the adaptation protocol, on the other hand, we preceded each test orientation with a fixed adapting orientation (-20° for 20 ms; Figure 6A).

Parameter Estimation and Plausibility Scores

The three models considered in this paper (C-model, M-model, and slow-model) all exhibit response properties (e.g., tuning width and time-to-peak) that resemble those observed experimentally in V1. We first performed an exhaustive search to find free parameters that generated single neuron responses we considered to be plausible based on the literature. For instance, for some model parameters neurons had peak firing rates of 200 spikes per second. Such responses are unusual in experimental recordings, hence, we assigned low plausibility scores to models that predicted such outcomes. An analogous scoring heuristic was applied based on single neuron's time-to-peak response and single neuron tuning widths.

To estimate these score functions, we fit kernel probability distributions to histograms of experimental data, using species-specific estimates where possible (Carandini and Ferster, 2000; DeValois et al., 1982; Gardner et al., 1999; Schummers et al., 2007; Wissig and Kohn, 2012). When more than one data set was available for the same experimental measure, we first normalized and summed the histograms before fitting the kernel distribution. The resulting distributions were then scaled to span the interval [0 1]. The scoring functions are shown in Figure S4. To score each model, we simulated the response to single gratings of all orientations, measured the time-to-peak, the peak response, and the tuning width, extracted the corresponding three scores from the three heuristic score functions, and averaged them to get a final plausibility score between zero and one. Note that plausibility as used here only refers to single stimulus responses, measured outside the context of an adaptation protocol.

This exhaustive search for plausible models was limited to parameters with the following values (minimum:stepsize:maximum): α = [4:1:13] Hz/mV; J_{lgn} = [7:1:16] mV/Hz; κ_{lgn} = [0.5:0.2:2.3]; J_{cortex} = [0.9:0.1:1.8] mV/Hz; r_{IE} = [1:0.02:1.18]; κ_E = [1.5:0.1:2.4]; κ_I = [1:0.1:1.9]; and τ was fixed to 15 ms during this exhaustive search. For every one of the 10^7 factorial combinations of these free parameters, we scored the resulting models according to the heuristic plausibility score and used the most plausible models (scores above 0.9) as initial estimates for an optimization procedure. The goal of this optimization

was to find parameters that best fit a specific set of experimental data obtained in an adaptation paradigm.

For each plausible initial guess, we determined the eight free parameters that matched the experimental data set most closely in the least-squares sense (*fmincon* in MATLAB). From this optimization, we selected the parameter sets with the lowest error and the highest plausibility score.

Optimization was done separately for data obtained in cat and macaque primary visual cortex. We refer to the best-fitting model for each of these data sets as the C-model and the M-model, respectively. The model fitting procedure was robust: we found large, contiguous parts of parameter space with a good match between the C-model and the data, as well as the M-model and the data. The time-to-peak, peak firing rate, and tuning width were well within the experimentally observed ranges for all model variants in the main text. The qualitative finding that recurrent networks generated repulsive shifts in tuning curves (Figure 6) was also robust: shifts in tuning curves were present, with different magnitudes and time courses, for all parameter sets that resulted in high plausibility scores.

For the C-model discussed in the main text, the eight free parameters were optimized to match adaptation in cat visual cortex (Felsen et al., 2002). This resulted in the following parameters: $\tau = 10.8$ ms; $\alpha = 10.6$ Hz/mV; $J_{lgn} = 9.57$ mV/Hz; $\kappa_{lgn} = 1.56$; $J_{cortex} = 1.71$ mV/Hz; $r_{IE} = 1.18$; $\kappa_E = 1.59$; and $\kappa_I = 1.16$. For the M-model, which was optimized to match adaptation in anaesthetized macaque visual cortex (Patterson et al., 2013), the parameters were: $\tau = 8$ ms; $\alpha = 3.88$ Hz/mV; $J_{lgn} = 11.04$ mV/Hz; $\kappa_{lgn} = 0.47$; $J_{cortex} = 2.84$ mV/Hz; $r_{IE} = 1.24$; $\kappa_E = 1.12$; and $\kappa_I = 0.56$.

For the model shown in Figure S1C, we fixed τ to 15 ms and then performed a random search through the remaining seven dimensional parameter space. This search was not exhaustive; we stopped the multiday search after finding several models with tuning curve shift time courses whose dynamics were on the order of s. The parameters of the exemplary slow model in Figure S1, panel C were: $\tau = 15$ ms; $\alpha = 4$ Hz/mV; $J_{lgn} = 8$ mV/Hz; $\kappa_{lgn} = 0.5$; $J_{cortex} = 1.7$ mV/Hz; $r_{IE} = 1.14$; $\kappa_E = 2.2$; and $\kappa_I = 1$, and its plausibility score was 0.4 if scored with cat plausibility and 0.6 if scored with anaesthetized monkey plausibility.

Experimental Data

Felsen et al. (2002) used single tungsten electrodes to record from neurons in primary visual cortex of anaesthetized cats. The grating stimuli were adjusted to match the optimal spatial frequency and receptive field size of the neuron under study. The stimuli were pairs or sequences of gratings in which each grating was presented for 25 ms or 17 ms. The time between two gratings was varied between 0 ms and 125 ms; the screen was blank during that period of time. We extracted the tuning curve shift data from their Figure 3B (based on the average tuning curve shift of 21 cells, reproduced here as Figure 2A). We extracted the time courses from their Figure 4B, which has separate time courses for 25 ms and 17 ms grating duration for a total of 20 cells. We also redefined "interval" to be the time (in milliseconds) that the screen was blank in between two oriented gratings. The model could be fit to either of these time courses (data not shown), but for simplicity we determined a single average time course by averaging the two curves (shown here in Figure 2C) and used the average stimulus duration (20 ms) for model simulations. We use C-model to refer to the best-fitting model for these data.

Patterson et al. (2013) used multielectrode arrays to record from neurons in layers 2/3 and 4B of the parafoveal representation in primary visual cortex of the anaesthetized macaque. The grating stimuli were adjusted to cover the aggregate receptive field of the neurons recorded by the electrode array, their spatial frequency was fixed at 1 cycle/°, and they drifted at 6.25 Hz. Of main interest here were their experiments that used a brief adaptor (400 ms) followed by a brief test (400 ms). Patterson et al. (2013) mapped the time course of tuning curve shifts by measuring the neural response in three separate epochs after test stimulus onset; early: 50–100 ms, mid: 100–200 ms, and late: 200–400 ms. We extracted the time course from their Figure 5C based on the average tuning curve shift of between 96 and 117 cells and compare it to model results in our Figure 2D. Because our model has no visual latency, we adjusted the time epochs to be 20–70 ms (early), 70–170 ms (mid), and 170–370 ms (late), assuming a visual latency for the data in Patterson et al. (2013) of 30 ms. We use "M-model" to refer to the best-fitting model for these data.

To simulate these experimental paradigms, we presented pairs of adapt/test gratings to the model. To replicate the Felsen et al. (2002) data, the adapting and test orientations were varied factorially, choosing from 12 equally distributed orientations between −90° and +90°. To replicate the Patterson et al. (2013) data, the adaptor had one of 13 equally distributed orientations between 15° and 75°, and the test one of 20 equally distributed orientations between −90° and +90°. From this data set, we extracted the tuning curves for each adaptor orientation. We also estimated tuning curves without an adaptor. The tuning curve shift was then calculated as the difference between the orientation at the peak of the adapted and non-adapted tuning curves.

SUPPLEMENTAL INFORMATION

Supplemental Information includes Supplemental Experimental Procedures and four figures and can be found with this article online at http://dx.doi.org/10.1016/j.celrep.2016.08.089.

AUTHOR CONTRIBUTIONS

Conceptualization, M.d.M.Q., A.P.M., and B.K.; Methodology, M.d.M.Q. and B.K.; Software, M.d.M.Q. and B.K.; Validation, M.d.M.Q. and B.K.; Formal Analysis, M.d.M.Q. and B.K.; Investigation, M.d.M.Q. and B.K.; Writing - Original Draft, M.d.M.Q. and B.K.; Writing - Review and Editing, B.K. and A.P.M.; Visualization, M.d.M.Q. and B.K.; Supervision, A.P.M. and B.K.; Project Administration, B.K.; and Funding Acquisition, B.K.

ACKNOWLEDGMENTS

We thank Denis Paré and Adam Kohn for their comments on the manuscript. This work was supported by the Charles and Johanna Busch Memorial Fund, the Pew Charitable Trusts, and the Eye Institute of the NIH (EY017605). The content is solely the responsibility of the authors and does not necessarily represent the official views of the NIH.

Received: February 25, 2016
Revised: June 25, 2016
Accepted: August 25, 2016
Published: September 27, 2016

REFERENCES

Angelucci, A., and Bressloff, P.C. (2006). Contribution of feedforward, lateral and feedback connections to the classical receptive field center and extra-classical receptive field surround of primate V1 neurons. Prog. Brain Res. *154*, 93–120.

Ben-Yishai, R., Hansel, D., and Sompolinsky, H. (1997). Traveling waves and the processing of weakly tuned inputs in a cortical network module. J. Comput. Neurosci. *4*, 57–77.

Benucci, A., Ringach, D.L., and Carandini, M. (2009). Coding of stimulus sequences by population responses in visual cortex. Nat. Neurosci. *12*, 1317–1324.

Borst, A., Flanagin, V.L., and Sompolinsky, H. (2005). Adaptation without parameter change: Dynamic gain control in motion detection. Proc. Natl. Acad. Sci. USA *102*, 6172–6176.

Bressloff, P.C., Bressloff, N.W., and Cowan, J.D. (2000). Dynamical mechanism for sharp orientation tuning in an integrate-and-fire model of a cortical hypercolumn. Neural Comput. *12*, 2473–2511.

Carandini, M., and Ringach, D.L. (1997). Predictions of a recurrent model of orientation selectivity. Vision Res. *37*, 3061–3071.

Carandini, M., and Ferster, D. (2000). Membrane potential and firing rate in cat primary visual cortex. J. Neurosci. *20*, 470–484.

Chung, S., and Ferster, D. (1998). Strength and orientation tuning of the thalamic input to simple cells revealed by electrically evoked cortical suppression. Neuron *20*, 1177–1189.

Clifford, C.W., Wyatt, A.M., Arnold, D.H., Smith, S.T., and Wenderoth, P. (2001). Orthogonal adaptation improves orientation discrimination. Vision Res. *41*, 151–159.

DeValois, R.L., Yund, E.W., and Hepler, N. (1982). The orientation and direction selectivity of cells in macaque visual cortex. Vision Res. *22*, 531–544.

Dragoi, V., Sharma, J., and Sur, M. (2000). Adaptation-induced plasticity of orientation tuning in adult visual cortex. Neuron *28*, 287–298.

Dragoi, V., Sharma, J., Miller, E.K., and Sur, M. (2002). Dynamics of neuronal sensitivity in visual cortex and local feature discrimination. Nat. Neurosci. *5*, 883–891.

Felsen, G., Shen, Y.S., Yao, H., Spor, G., Li, C., and Dan, Y. (2002). Dynamic modification of cortical orientation tuning mediated by recurrent connections. Neuron *36*, 945–954.

Ferster, D., and Miller, K.D. (2000). Neural mechanisms of orientation selectivity in the visual cortex. Annu. Rev. Neurosci. *23*, 441–471.

Gardner, J.L., Anzai, A., Ohzawa, I., and Freeman, R.D. (1999). Linear and nonlinear contributions to orientation tuning of simple cells in the cat's striate cortex. Vis. Neurosci. *16*, 1115–1121.

Gibson, J.J., and Radner, M. (1937). Adaptation, aftereffect and contrast in the perception of tilted lines: I. Quantitative studies. J. Exp. Psychol. *20*, 453–467.

Gilbert, C.D., and Wiesel, T.N. (1990). The influence of contextual stimuli on the orientation selectivity of cells in primary visual cortex of the cat. Vision Res. *30*, 1689–1701.

Hahnloser, R.H.R., Douglas, R.J., and Hepp, K. (2002). Attentional recruitment of inter-areal recurrent networks for selective gain control. Neural Comput. *14*, 1669–1689.

Hansel, D., and Sompolinsky, H. (1998). Modeling feature selectivity in local cortical circuits. In Methods in Neuronal Modeling: From Ions to Networks, C. Koch and I. Segev, eds. (Boston, MA: MIT Press), pp. 499–567.

Hubel, D.H., and Wiesel, T.N. (1962). Receptive fields, binocular interaction and functional architecture in the cat's visual cortex. J. Physiol. *160*, 106–154.

Ibbotson, M., and Krekelberg, B. (2011). Visual perception and saccadic eye movements. Curr. Opin. Neurobiol. *21*, 553–558.

Joukes, J., Hartmann, T.S., and Krekelberg, B. (2014). Motion detection based on recurrent network dynamics. Front. Syst. Neurosci. *8*, 239.

Kar, K., and Krekelberg, B. (2016). Testing the assumptions underlying fMRI adaptation using intracortical recordings in area MT. Cortex *80*, 21–34.

Kaschube, M. (2014). Neural maps versus salt-and-pepper organization in visual cortex. Curr. Opin. Neurobiol. *24*, 95–102.

Ko, H., Hofer, S.B., Pichler, B., Buchanan, K.A., Sjöström, P.J., and Mrsic-Flogel, T.D. (2011). Functional specificity of local synaptic connections in neocortical networks. Nature *473*, 87–91.

Krekelberg, B., Boynton, G.M., and van Wezel, R.J.A. (2006a). Adaptation: from single cells to BOLD signals. Trends Neurosci. *29*, 250–256.

Krekelberg, B., van Wezel, R.J.A., and Albright, T.D. (2006b). Adaptation in macaque MT reduces perceived speed and improves speed discrimination. J. Neurophysiol. *95*, 255–270.

Kristjánsson, Á. (2011). The functional benefits of tilt adaptation. Seeing Perceiving *24*, 37–51.

Michalski, A., Gerstein, G.L., Czarkowska, J., and Tarnecki, R. (1983). Interactions between cat striate cortex neurons. Exp. Brain Res. *51*, 97–107.

Müller, J.R., Metha, A.B., Krauskopf, J., and Lennie, P. (1999). Rapid adaptation in visual cortex to the structure of images. Science *285*, 1405–1408.

Patterson, C.A., Wissig, S.C., and Kohn, A. (2013). Distinct effects of brief and prolonged adaptation on orientation tuning in primary visual cortex. J. Neurosci. *33*, 532–543.

Patterson, C.A., Duijnhouwer, J., Wissig, S.C., Krekelberg, B., and Kohn, A. (2014). Similar adaptation effects in primary visual cortex and area MT of the macaque monkey under matched stimulus conditions. J. Neurophysiol. *111*, 1203–1213.

Priebe, N.J., and Ferster, D. (2008). Inhibition, spike threshold, and stimulus selectivity in primary visual cortex. Neuron *57*, 482–497.

Richert, M., Albright, T.D., and Krekelberg, B. (2013). The complex structure of receptive fields in the middle temporal area. Front. Syst. Neurosci. *7*, 2.

Roerig, B., and Chen, B. (2002). Relationships of local inhibitory and excitatory circuits to orientation preference maps in ferret visual cortex. Cereb. Cortex *12*, 187–198.

Rutishauser, U., and Douglas, R.J. (2009). State-dependent computation using coupled recurrent networks. Neural Comput. *21*, 478–509.

Sanchez-Vives, M.V., Nowak, L.G., and McCormick, D.A. (2000). Membrane mechanisms underlying contrast adaptation in cat area 17 in vivo. J. Neurosci. *20*, 4267–4285.

Schlack, A., Krekelberg, B., and Albright, T.D. (2007). Recent history of stimulus speeds affects the speed tuning of neurons in area MT. J. Neurosci. *27*, 11009–11018.

Schummers, J., Cronin, B., Wimmer, K., Stimberg, M., Martin, R., Obermayer, K., Koerding, K., and Sur, M. (2007). Dynamics of orientation tuning in cat v1 neurons depend on location within layers and orientation maps. Front. Neurosci. *1*, 145–159.

Schwabe, L., Obermayer, K., Angelucci, A., and Bressloff, P.C. (2006). The role of feedback in shaping the extra-classical receptive field of cortical neurons: a recurrent network model. J. Neurosci. *26*, 9117–9129.

Schwartz, O., Hsu, A., and Dayan, P. (2007). Space and time in visual context. Nat. Rev. Neurosci. *8*, 522–535.

Shushruth, S., Mangapathy, P., Ichida, J.M., Bressloff, P.C., Schwabe, L., and Angelucci, A. (2012). Strong recurrent networks compute the orientation tuning of surround modulation in the primate primary visual cortex. J. Neurosci. *32*, 308–321.

Somers, D.C., Nelson, S.B., and Sur, M. (1995). An emergent model of orientation selectivity in cat visual cortical simple cells. J. Neurosci. *15*, 5448–5465.

Sompolinsky, H., and Shapley, R. (1997). New perspectives on the mechanisms for orientation selectivity. Curr. Opin. Neurobiol. *7*, 514–522.

Teich, A.F., and Qian, N. (2003). Learning and adaptation in a recurrent model of V1 orientation selectivity. J. Neurophysiol. *89*, 2086–2100.

Wilson, H.R., and Cowan, J.D. (1972). Excitatory and inhibitory interactions in localized populations of model neurons. Biophys. J. *12*, 1–24.

Wissig, S.C., and Kohn, A. (2012). The influence of surround suppression on adaptation effects in primary visual cortex. J. Neurophysiol. *107*, 3370–3384.

Yao, H., and Dan, Y. (2001). Stimulus timing-dependent plasticity in cortical processing of orientation. Neuron *32*, 315–323.

Cell Reports, Volume *17*

Supplemental Information

Adaptation without Plasticity

Maria del Mar Quiroga, Adam P. Morris, and Bart Krekelberg

Adaptation without Plasticity

Supplementary Materials

Maria del Mar Quiroga[1,2], Adam P. Morris[3], and Bart Krekelberg[1]

[1] Center for Molecular and Behavioral Neuroscience, Rutgers University – Newark, New Jersey, 07102, USA.

[2] Behavioral and Neural Sciences Graduate Program, Rutgers University – Newark, New Jersey, 07102, USA.

[3] Neuroscience Program, Biomedicine Discovery Institute, Department of Physiology, Monash University, Clayton, Victoria 3800, Australia.

Correspondence to: Bart Krekelberg (bart@vision.rutgers.edu)

Supplemental Figures

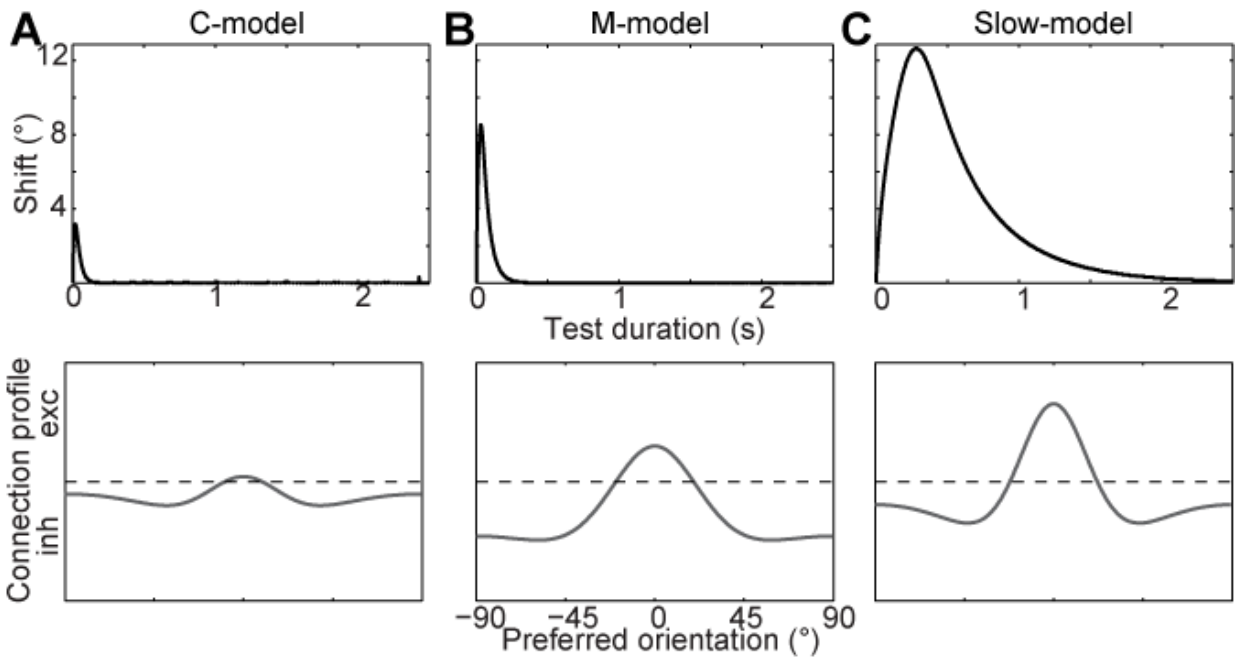

Figure S1. *The relation between intracortical connection profiles and the magnitude and dynamics of tuning curve shifts. Related to Figure 3.* ***A)*** *C-model.* ***B)*** *M-model.* ***C)*** *Slow-model. The top panels show the magnitude of the shift in the tuning curve as a function of time after test stimulus onset. The tuning curves were obtained by averaging the response for the whole duration of the test stimulus. These panels show that tuning curve shifts on the order of several degrees and a time scale of seconds can be explained by a recurrent network model and do not require plastic network changes. The bottom panels show the intracortical connection profile for the neuron with preferred orientation 0°. The parameters of the slow model were chosen to generate slow but still V1-like response properties and tuning by a random search through all possible models, while keeping the neurons' membrane time constant τ = 15 ms (See Experimental Procedures). This shows that the intracortical connection profile plays an important role in the generation of slow dynamics.*

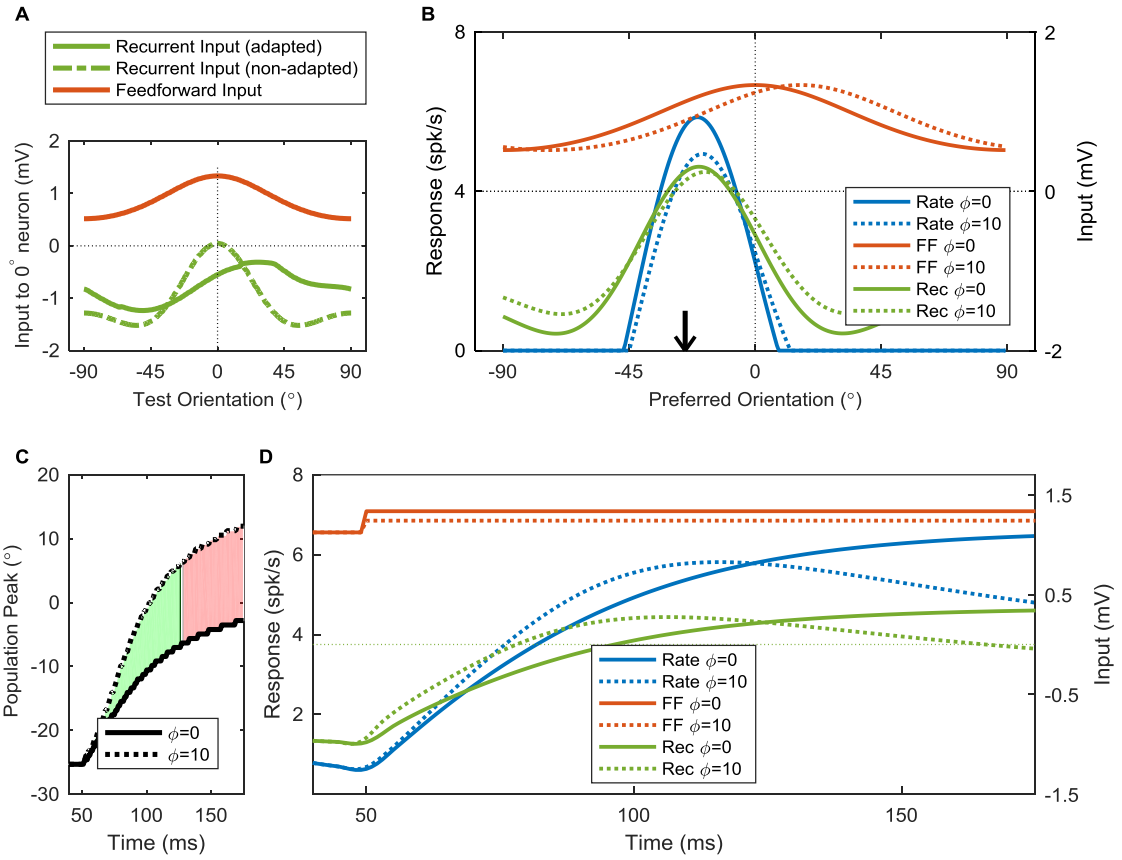

Figure S2. *Mechanisms; the influence of the tuning of excitatory connections. Related to Figure 7. Detailed simulation of an adaptation protocol in the M-model. All parameters were identical to those used for Figure 7, except for the tuning of the excitatory connections which was narrower (stretch factor = 0.83). All graphical conventions are the same as Figure 7.* ***A)*** *Input to the neuron that nominally prefers 0° as a function of test stimulus orientation.* ***B)*** *Population activity and input immediately after the onset of the test stimulus (t=65 ms).* ***C)*** *Dynamics of the hill of population activity.* ***D)*** *Dynamics of the input and response of the 0° neuron. Compared to the simulation in Figure 7, the narrower excitatory connections result in a narrower hill of activity (blue lines in panel B), which results in a larger difference between the recurrent excitation generated by the 0° and 10° test stimulus (solid green vs. dashed green curve in panel B and D), and therefore a larger difference in the firing rate for the 10° compared to the 0° test stimulus (dashed versus solid curve in panel D). As a consequence, even a test stimulus with an orientation larger than 10° will briefly generate a bigger response than the 0° and 10° stimulus and temporarily become the preferred stimulus. This illustrates how narrower excitatory connectivity results in larger tuning curve shifts.*

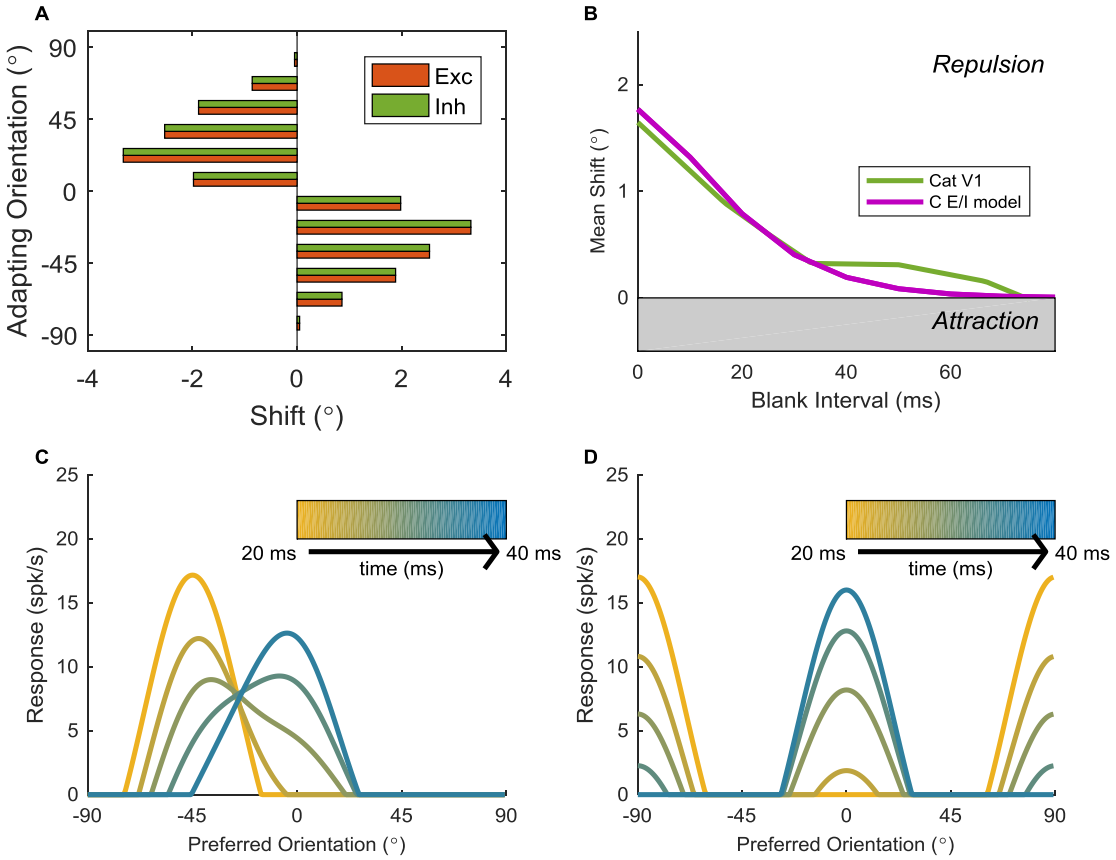

Figure S3. *Simulation results of the E/I model. Related to Figure 2 and 5. This model extends the model used in the main text by using separate populations of excitatory and inhibitory cells. Neurons in these populations are connected within the population (EE and II) and across (EI, IE) through lateral weights with a von Mises shape (Supplemental Experimental Procedures). Model parameters matched those of the C-model in the main text. For simplicity we assumed the tuning of the excitatory and inhibitory connections to be the same irrespective of their excitatory or inhibitory targets (* $\kappa_{EI} = \kappa_{EE}$ *and* $\kappa_{II} = \kappa_{IE}$ *). Given this choice, E and I populations behave identically in terms of dynamics and tuning curve shifts.* ***A)*** *Tuning curve shifts for the excitatory (red) and inhibitory (green) neuron with preferred orientation 0°; the analysis is identical to that for the single population model in Figure 2B.* ***B)*** *Time course of tuning curve shifts. Analysis identical to that in Figure 2C.* ***C)*** *Population dynamics for a -45° adapter followed by a 0° test, both presented for 20 ms. Line color represents time since start of the simulation as shown in the color bar. Analysis matches that of Figure 6B.* ***D)*** *Simulation of the population dynamics for a -90° adapter, followed by a 0° test, both presented for 20 ms. Analysis matches that of figure 5D. This figure shows that tuning curve shifts and their dynamics can be found in a network that respects the categorical difference between excitatory and inhibitory neurons.*

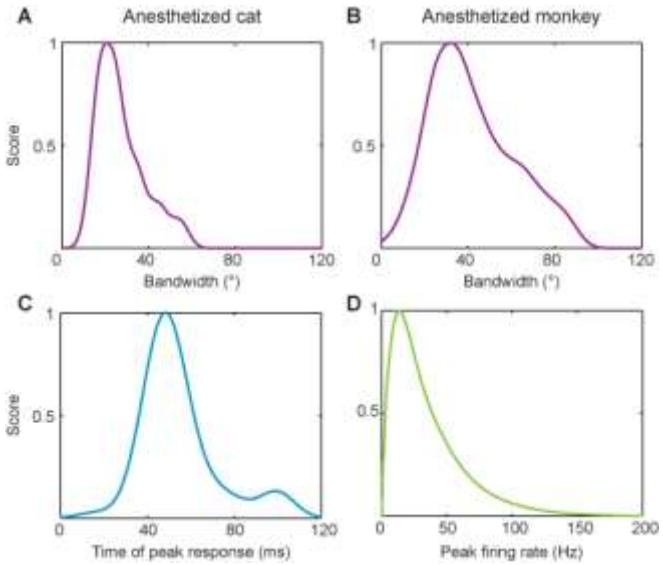

Figure S4*. Heuristic plausibility scoring functions, estimated from the experimental literature. Related to Experimental Procedures in the main text. These scoring functions were used to constrain model parameters such that only models with plausible tuning widths, dynamics, and peak firing were considered (See Experimental Procedures in main text).* ***A)*** *Scoring function for tuning curve bandwidth; based on anaesthetized cat recordings* (Gardner et al. 1999; Carandini & Ferster 2000)*.* ***B)*** *Tuning bandwidth score for anaesthetized monkey recordings* (DeValois et al. 1982)*.* ***C)*** *Time-to-peak score based on anaesthetized cat recordings* (Schummers et al. 2007)*.* ***D)*** *Peak firing rate score based on anaesthetized monkey recordings* (Wissig & Kohn 2012)*.*

Supplemental Experimental Procedures

The two population model of **Figure S3** is a straightforward generalization of the one-population model used in the main text (Wilson & Cowan 1972; Ben-Yishai et al. 1995). We use the subscript x to index the populations of excitatory ($x = E$) and inhibitory ($x = I$) neurons. The membrane potential dynamics are:

$$\tau \frac{dV_x^{\theta}}{dt} + V_x^{\theta} = V_{\lg n}^{\theta} + V_{x,cortex}^{\theta}$$

and the firing rate:

$$R_x^{\theta}(t) = \alpha \max\left(V_x^{\theta}(t), 0\right).$$

The recurrent input is determined as:

$$V_{x,cortex}^{\theta}(t) = J_{x,cortex}\left(\sum_{\varphi} f(\varphi \mid \theta, \kappa_{Ex}) R_E^{\varphi}(t) - r_{x,IE} f(\varphi \mid \theta, \kappa_{Ix}) R_I^{\varphi}(t)\right)$$

With f a von Mises function (See Experimental Procedures). The concentration parameter of the von Mises function determines the tuning of excitatory to excitatory (κ_{EE}), excitatory to inhibitory (κ_{EI}), inhibitory to inhibitory (κ_{II}), and inhibitory to excitatory connections (κ_{IE}). The parameters $J_{E,cortex}$ and $J_{I,cortex}$ set the overall strength of recurrent input compare to the feedforward input, and the parameters $r_{E,IE}$ and $r_{I,IE}$ set the balance of excitation and inhibition. For the simulation in **Figure S3** the free parameters were matched to those of the C-model in the main text: τ = 10.8 ms; α = 10.6 Hz/mV; $J_{\lg n}$ = 9.57 mV/Hz; $\kappa_{\lg n}$ = 1.56; $J_{E,cortex} = J_{I,cortex}$ =1.71 mV/Hz; $r_{E,IE} = r_{I,IE}$ = 1.18; $\kappa_{EI} = \kappa_{EE}$ = 1.59; $\kappa_{II} = \kappa_{IE}$ = 1.16.

Supplemental References

Ben-Yishai, R., Bar-Or, R.L. & Sompolinsky, H., 1995. Theory of orientation tuning in visual cortex. Proceedings of the National Academy of Sciences, USA, 92, pp.3844–3848.

Carandini, M. & Ferster, D., 2000. Membrane potential and firing rate in cat primary visual cortex. Journal of Neuroscience, 20, pp.470–484.

DeValois, R.L., Yung, E.W. & Hepler, N., 1982. The orientation and direction selectivity of cells in macaque visual cortex. Vision Research, 22, pp.531–544.

Gardner, J.L. et al., 1999. Linear and nonlinear contributions to orientation tuning of simple cells in the cat's striate cortex. Visual Neuroscience, 16, pp.1115–1121.

Schummers, J. et al., 2007. Dynamics of orientation tuning in cat v1 neurons depend on location within layers and orientation maps. Frontiers in Neuroscience, 1, pp.145–159.

Wilson, H.R. & Cowan, J.D., 1972. Excitatory and inhibitory interactions in localized populations of model neurons. Biophysical journal, 12(1), pp.1–24.

Wissig, S.C. & Kohn, A., 2012. The influence of surround suppression on adaptation effects in primary visual cortex. Journal of Neurophysiology, 107(12), pp.3370–3384.